CHAPTER CONTENTS

CHAPTER 3. AIRCRAFT-BASED OBSERVATIONS

3.1 GENERAL

3.1.1 Definitions

This chapter describes the methods used for automatic meteorological measurements on modern commercial aircraft, known collectively as aircraft-based observations. The principles described here may be used for data processing on any adequately instrumented aircraft to define and develop aircraft-based observing systems.

The WMO aircraft meteorological data relay (AMDAR) observing system is an aircraft-based observing system that is specified in WMO (2013) so as to meet meteorological requirements for reporting meteorological data from an aircraft platform. The AMDAR system is operated by WMO Members in collaborative agreement with their partner airlines, and the resulting data are transmitted on the WMO Global Telecommunication System. Additional information is available in WMO (2003).

AMDAR and other aircraft-based observing systems are generally implemented on aircraft that are equipped with sophisticated navigation and other sensing systems. There are sensors for measuring airspeed, air temperature and air pressure. Other data relating to aircraft position, acceleration and orientation are available from the aircraft navigation system. The aircraft also carry airborne computers for the flight management and navigation systems, by which navigation and meteorological data are computed continuously and are made available to the aircrew at the flight deck. In aircraft-based observing systems, they are further processed and fed automatically to the aircraft communication system for transmission to the ground, or, alternatively, a dedicated processing package can be used on the aircraft to access raw data from the aircraft systems and derive the meteorological variables independently.

In AMDAR systems, these facilities are used to compile and transmit meteorological reports in real time. Normally, the messages contain wind speed and direction (in the horizontal plane), air temperature, pressure altitude (altitude in the Standard Atmosphere related to a reference pressure level), time of observation, phase of flight and the aircraft position. If the aircraft is properly equipped, it may also report humidity or water vapour mixing ratio and a measure of turbulence.

The source data for meteorological observations require significant correction and complex processing to yield meteorological measurements that are representative of the free air-stream in the aircraft vicinity. A full description of all the processes involved is beyond the scope of this Guide, but an outline of the principles is given here, with references for further reading.

3.1.2 Aircraft meteorological sensors

The basic sensors carried on modern commercial aircraft comprise the pitot-static probe and the total air temperature (TAT) probe. Data from these sensors, together with information from the aircraft navigation system, usually provided by one or a combination of radio navaid systems (Global Positioning System, GPS), distance-measuring equipment (DME), VHF omni-directional radio range (VOR), an instrument landing system and in some cases an inertial navigation system (INS), are processed to give the following meteorological elements:

(a) Pressure altitude H_p,[1] horizontal position and time (PALT in Figure 3.1);

(b) Static air temperature T_s (SAT in Figure 3.1);

(c) Wind speed |V|;

(d) Wind direction D_w.

On some aircraft, additional processing for measuring turbulence is available or additional sensors are available for measuring ice build-up on the front surfaces and/or for measuring relative humidity or water vapour mixing ratio *r*.

In order to appreciate the complexity of the processing system, the following description is structured according to the process flow in a typical operational system. It will be noted (Figure 3.1) that the computed variables are highly interdependent.

3.2 PRESSURE AND MACH NUMBER

3.2.1 Pitot-static probe

The pitot-static probe (Figure 3.2) is exposed in the free air-stream beyond the aircraft boundary layer and provides the total pressure (static pressure plus impact or dynamic pressure). Some of these sondes can provide static pressure as well (i.e. free air-stream pressure, ideally the undisturbed ambient pressure), but on most airliners normally in use for AMDAR, the static pressure is provided via orifices on the side of the aircraft body. The pressure values are measured by electronic transducers and passed to a central unit hosting the algorithms for the aerodynamic adjustments (correction for the built-in error) and finally to the air data computer (ADC). The ADC computes pressure altitude, static temperature and Mach number from these two measurements.

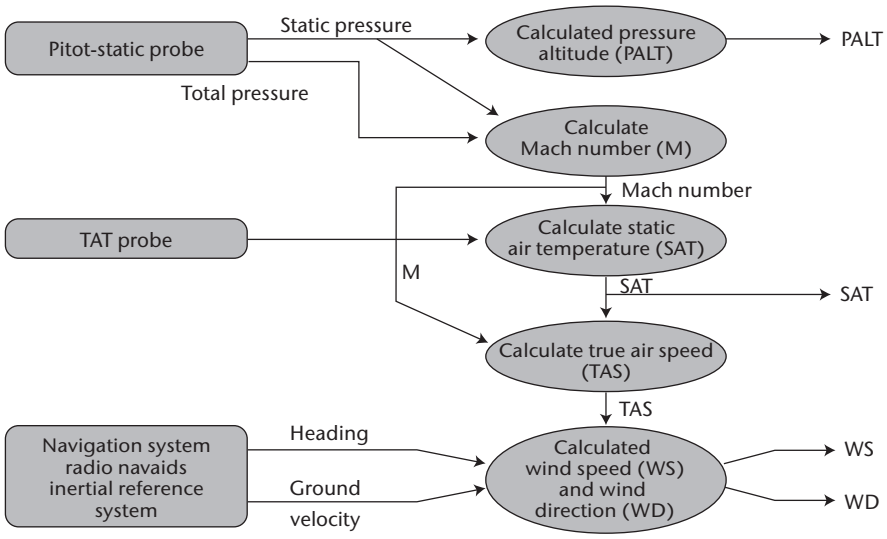

Figure 3.1. AMDAR sensor data processing

[1] Pressure altitude is defined as a measure of height relative to the standard datum plane of 1 013.2 hPa. The variable flight level (FL) equals the pressure altitude for all levels. Pressure altitude and flight level may not be interchanged with indicated aircraft altitude, aircraft altitude, or aircraft height, for which other definitions apply. Because aircraft may fly at pressure levels above 1 013.2 hPa (i.e. below the standard datum plane), pressure altitude (or flight level) may be negative.

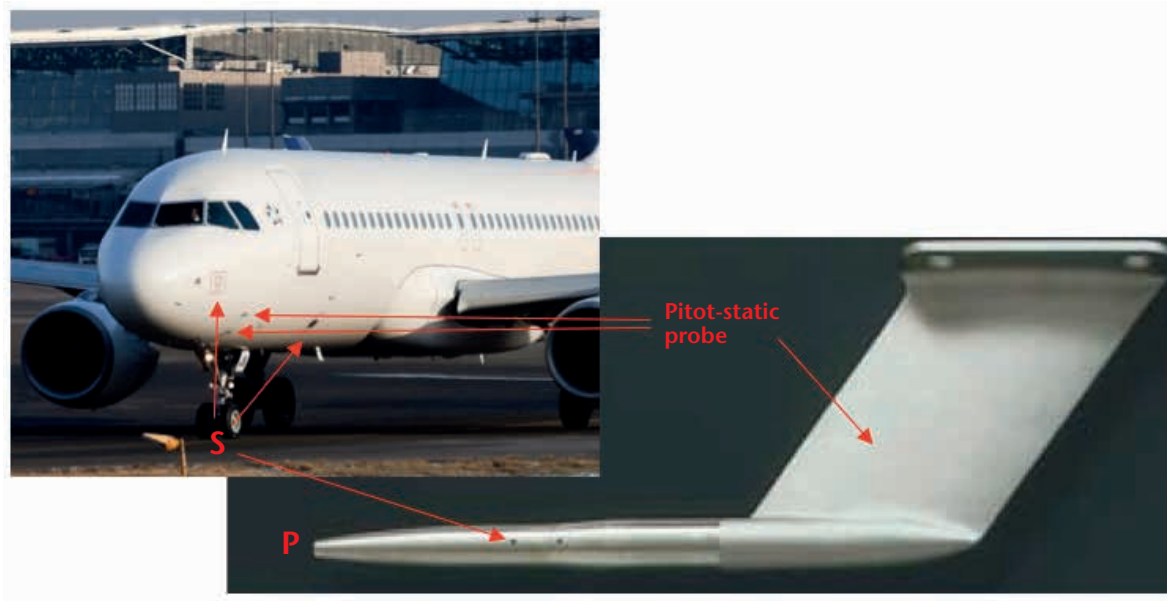

Figure 3.2. Typical configuration for the measurement of static pressure and pitot pressure on aircraft. Static pressure is taken (see the mark "S") either at ports on both sides of the fuselage or at side ports of the pitot-static probe. Total pressure is taken at the forward-headed orifice of the pitot probes or the pitot-static probes (see the mark "P") mounted on the fuselage a few metres behind the nose.

3.2.2 Pressure altitude

The static pressure measurement is not normally reported in AMDAR but is converted in the ADC to the equivalent altitude based on the International Standard Atmosphere (ISO, 2007). The Standard Atmosphere (see Figure 3.3) assumes a linear decrease in temperature with height of 6.5 °C per km up to 11 km or 36 089 ft,[2] and a mean sea-level temperature and pressure of 15 °C and 1 013.25 hPa, respectively. From 11 km to 20 km the temperature is assumed constant at –56.5 °C.

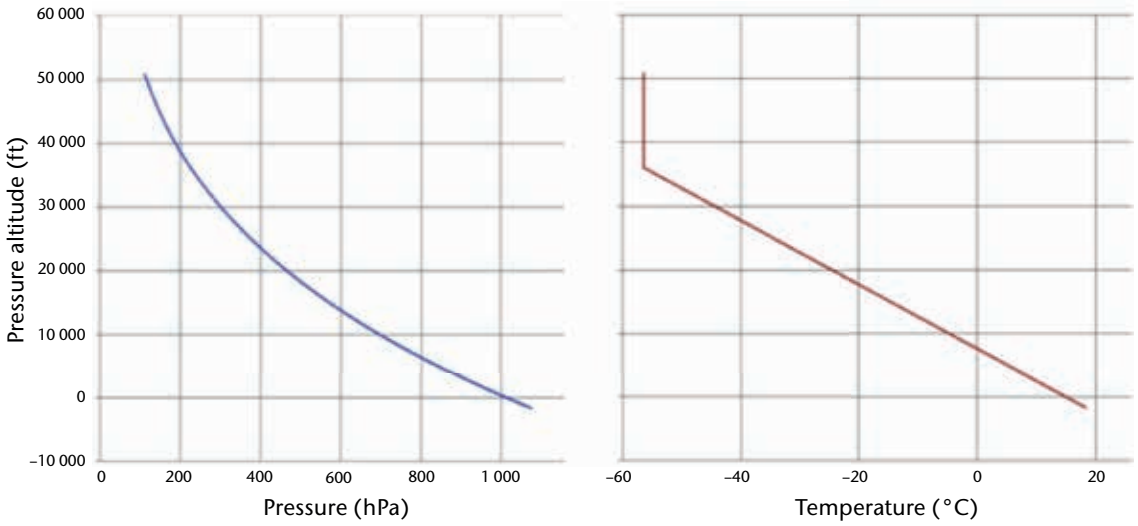

Figure 3.3. International Standard Atmosphere

[2] Despite the general policy to use SI units, feet are used for altitude in this chapter, respecting common practice in the aviation community.

For pressure altitude H_p equal to or less than 36 089 ft, static pressure (p_s) is related to H_p by the following expression:

$$p_S = 1\,013.25 \cdot \left(1 - 6.8756 \cdot 10^{-6} \cdot H_p\right)^{5.2559} \tag{3.1}$$

with H_p in units of ft and p_s in units of hPa. For example, if H_p is 30 000 ft, p_s = 300.9 hPa.

The above expression (3.1) can be used to calculate the static pressure from the reported pressure altitude, provided that the on-board static pressure value was corrected only for aerodynamically-induced effects (built-in error) and the aircraft altimeter sub-scale (zero-reference) was set to ICAO standard mean sea level pressure (1 013.25 hPa). Navigational procedures also provide for altimeter sub-scale settings at other reference levels. For example, the setting can be aerodrome pressure (field elevation pressure, QFE) or QNH (QFE value reduced to sea level by use of the Standard Atmosphere), which is a pressure reference on the standard atmosphere scale such that aerodrome height is indicated at touchdown on a specific airfield. The pressure altitude reported by the AMDAR on-board software should always be with respect to ICAO mean sea level pressure only.

For use in the cockpit, the indicated altitude H_i (the pressure altitude above mean sea level (MSL)) is given by the pressure altitude (H_p) minus the altitude of the altimeter sub-scale reference on the standard atmosphere scale (H_r) plus the elevation of the reference pressure level above MSL (E_{Ref}). The general expression is:

$$H_i = H_p - H_r + E_{\text{Ref}} \tag{3.2}$$

$$H_r = \left[1 - \left(\frac{p_r}{1\,013.25}\right)^{0.190\,26}\right] \cdot 145\,442 \tag{3.3}$$

with H_r, H_i, and E_{Ref} in units of ft, and p_r in units of hPa; p_r is the altimeter sub-scale setting, such as:

QNH, then E_{Ref} = 0 ft above mean sea level

or

QFE, then E_{Ref} = field elevation above mean sea level

Note that H_r = 0 if p_r = 1 013.25 hPa.

For example:

(a) If the sub-scale setting is a QNH value of 1 000.0 hPa and the indicated altitude is 9 335 ft, H_p = 9 335 ft + 364 ft = 9 699 ft and p_s = 705 hPa;

(b) If the sub-scale setting is a QFE value of 990 hPa, the aerodrome height is 276 ft and the indicated altitude is 9 058 ft, $H_p = H_i + H_r$ (QFE) – E_{Ref} = 9 058 ft + 641 ft – 276 ft = 9 423 ft and the QNH value would be 1 000 hPa.

However, for the purpose of AMDAR, the altitude parameter should be chosen which is solely based on the aerodynamically clean static pressure without any reference to QNH or QFE.

If H_p is greater than 36 089 ft (11 km), static pressure is given by:

$$p_S = 226.32 \cdot e^{\frac{36\,089 - H_p}{20\,806}}$$

or (3.4)

$$H_p = 36\,089 - 20\,806 \cdot \ln\left(\frac{p_S}{226.32}\right)$$

with H_p in units of ft, and p_s in units of hPa. For example, if H_p is 40 000 ft, p_s = 187.5 hPa.

3.2.2.1 *Measurement uncertainty*

Sources of uncertainty include:

(a) Calibration uncertainty;

(b) Short-term random instrument error;

(c) Calibration drift;

(d) Exposure uncertainty or static source uncertainty (built-in).

Because aircraft safety separations are critical, these uncertainties are corrected for as much as possible in the ADC. Static source uncertainty, which is a function of probe location, Mach number and aircraft weight, is determined empirically during flight-testing. Uncertainty of pressure is inferred from reported heights.

A possible source of data latency with the AMDAR system is in the radio link between aircraft and ground. This link process is regulated by international standards, such as ARINC 620, AOSFRS (AMDAR Onboard Software Functional Requirements Specification) or AAA, which stands for ACMS (Aircraft Condition Monitoring System) ACARS AMDAR. In earlier versions of these standards, the pressure altitudes were reported in hundreds of feet, equivalent at cruise level to some 1.5 hPa. This represents roughly 0.1% of the full scale pressure measurement. With instrumental accuracy at best of the order of 1 hPa, the uncertainty in static pressure at cruise level derived from converting pressure altitude is about 2 hPa. At zero reference level, the resolution is equivalent to about 3.7 hPa, leading to an uncertainty of some 4 hPa. In recent versions of the AMDAR on-board software, the altitude is reported in tens of feet, in which case the uncertainty due to coding-related error is lower than the remainder of the measurement uncertainty. AMDAR-equipped aircraft meet the rules and requirements of Reduced Vertical Separation Minima (RVSM) as laid down by the approved authorities within Air Traffic Management (ATM). The aircraft are required to maintain an altitude uncertainty of 50 m (160 ft), even in the altitude range of 30 000 to 40 000 ft. Hence, the pressure uncertainty has to be within the range of ±1.5 hPa and the quality control system of the airline must maintain this level of accuracy.

3.2.3 Mach number

Mach number (M, the true airspeed divided by the speed of sound in the free air) is an important element for aircraft operations. In AMDAR systems, it is used to correct air-temperature measurements and airspeed measurements. In dry air, the speed of sound is proportional to the square root of absolute (static) temperature T_s. Mach number only depends on two parameters:

(a) The impact pressure q_c measured by the aircraft's pitot tubes; and

(b) The static pressure p_s measured at specific locations on the side of the aircraft fuselage:

$$M^2 = \frac{2}{\kappa - 1}\left[\left(\frac{q_c + p_s}{p_s}\right)^{\frac{\kappa-1}{\kappa}} - 1\right] \tag{3.5}$$

where $q_c + p_s$ is the total pressure, and κ is the ratio of specific heats of dry air (C_p/C_v).

For further details, see the standard texts on aircraft aerodynamics such as Abbott and von Doenhoff (1959) and Dommasch et al. (1958).

3.2.3.1 *Measurement uncertainty*

The measurement uncertainty is determined almost entirely by the uncertainty of the fundamental measurements of pressure. In normal operation, the derived Mach number uncertainty should be lower than 0.2%.

3.3 AIR TEMPERATURE

3.3.1 Total air temperature probe

The TAT probe is exposed in the free air-stream and used to derive static (free air-stream) temperature. The accurate measurement of air temperature is fundamental to the other derived meteorological elements. For example, it is used in the calculation of true airspeed and thus has an impact on the calculation of the wind velocity components. The ADC corrects the temperature actually measured by the probe using the computed Mach number.

Most commercial aircraft are equipped with TAT probes of the immersion thermometer type. Figure 3.4 shows a typical example. The sensing element is a resistance thermometer. The housing is designed to divert cloud and precipitation hydrometeors from the sensing element, although it has been reported (Lawson and Cooper, 1990) that the sensing element becomes wet in cumulus clouds. However, the main reason for the aerodynamic particle separation is to protect the element against abrasive impacts.

The thermodynamically important part of the housing's design is to achieve for the sampled air a nearly complete adiabatic conversion of its kinetic energy into internal energy. The airspeed has to be reduced to a leftover of a few m/s at the sensor. At this location, the air-stream getting in contact with the sensitive element must have been kept free of heat exchange with the internal walls. That is why all the different kinds of TAT housings are equipped/designed with holes in the walls around the intake flow. These holes produce an aerodynamic sucking effect to curb the

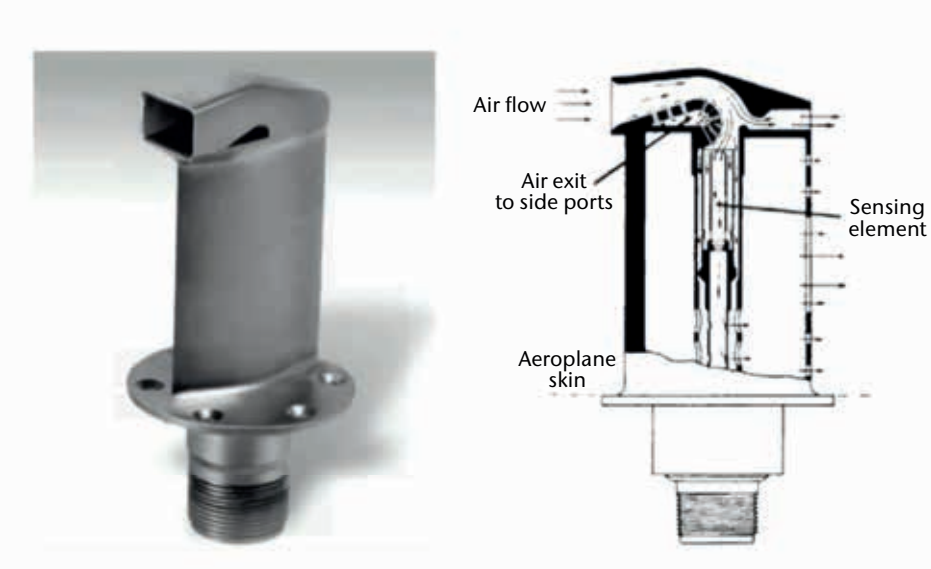

Figure 3.4. Typical example of an aircraft temperature sensor: a total air temperature probe. The internal aerodynamics is designed to make the flow stagnate before touching the sensor. The associated internal boundary-layer is kept small enough and away from the sensor element to enable a pure adiabatic process. The flow's curvature serves for particle separation.

internal boundary layer. As a result, the heat exchange with the wall is kept sufficiently small to maintain accuracy of the measurements. Even if the housing's intake edge is heated for de-icing, the associated increase of the measured temperature is below 0.5 K at $M > 0.3$.

The temperature (T_r) measured by the probe is close to the theoretical value of T_t that would occur with perfect adiabatic compression of the free air-stream at an aerodynamically ideal stagnation point. The static air temperature T_s, which is the temperature of the free air-stream, is related to the measured temperature T_r by the expression (with T as absolute temperature):

$$\frac{T_r}{T_s} = 1 + \lambda \cdot \frac{\kappa - 1}{2} \cdot M^2 \tag{3.6}$$

where λ is the probe recovery factor. Modern TAT probes show typical values of the probe recovery factor around 0.98 for Mach numbers between 0.5 and 0.9. It primarily includes the effect of incomplete stagnation of air and, secondarily, that of a small frictional heat transfer to the flow to be sampled. The value of this coefficient is slightly smaller than 1. It depends on the housing's design but also on the Mach number. At cruise level at Mach 0.85, the probe temperature exceeds the ambient temperature by more than 30 K.

Further details about TAT probes can be found in Stickney et al. (1990).

3.3.1.1 *Measurement uncertainty*

The static temperature is a function of probe temperature and Mach number. As shown above, the Mach number is derived from total pressure and static pressure, themselves independent measurements from the pitot-static head. The uncertainty of measurement is therefore a function of three error sources in addition to calibration uncertainties and other effects (for example, probe de-icing).

The temperature uncertainty is about 0.4 °C at Mach 0.8, reducing to 0.3 °C at low Mach numbers. In the first version of the on-board software standard ARINC 620, the temperature had a resolution of 1 K. Since 1994, it has been specified to be coded in 0.1 K. If the sensor is wetted in cloud, it will be cooled by evaporation leading to additional uncertainties up to 3 °C or so. At very low airspeed (for example prior to take-off) there may be insufficient airflow over the sensor to maintain the accuracy of measurement. Some aircraft employ aspirated sensors to overcome this problem. Normally the on-board software should be configured so that a data transfer does not begin before take-off. Despite the complexity of the data processing involved, operational experience suggests that mean-temperature uncertainty at cruise height is about 1 K.

3.4 WIND SPEED AND DIRECTION

The measurement of the three-dimensional wind vector uses data from the aircraft navigation system (the complete combination or a subset of a radio navaid, inertial platform, magnetic compass and GPS system) and the airspeed system (air data computer using pitot-static system plus TAT probe). Using these data, it is possible to calculate to a high degree of accuracy the velocity (V_g) of the aircraft, the ground speed with respect to the Earth and the aircraft velocity with respect to the air (V_a, true airspeed). The wind vector (V), therefore, is given by the vector triangle:

$$\vec{v} = \vec{v}_g - \vec{v}_a \tag{3.7}$$

The vectors $\vec{v}_g$ and $\vec{v}_a$ must be measured accurately since typical horizontal winds are small

(some 10 m/s) compared with aircraft ground speed and true airspeed (200 to 300 m/s). In early AMDAR systems during long-range navigation the ground speed was derived solely from inertial navigation systems without any support of ground-based navaids or GPS. Sometimes this may have reduced the accuracy of the ground-speed vector and the wind vector by some m/s. This has been improved with modern multi-sensor navigation systems in order to produce operational quality data (Meteorological Service of Canada, 2003). However, the three-dimensional solution of the vector (equation 3.7) needs the measurements of aircraft pitch, roll

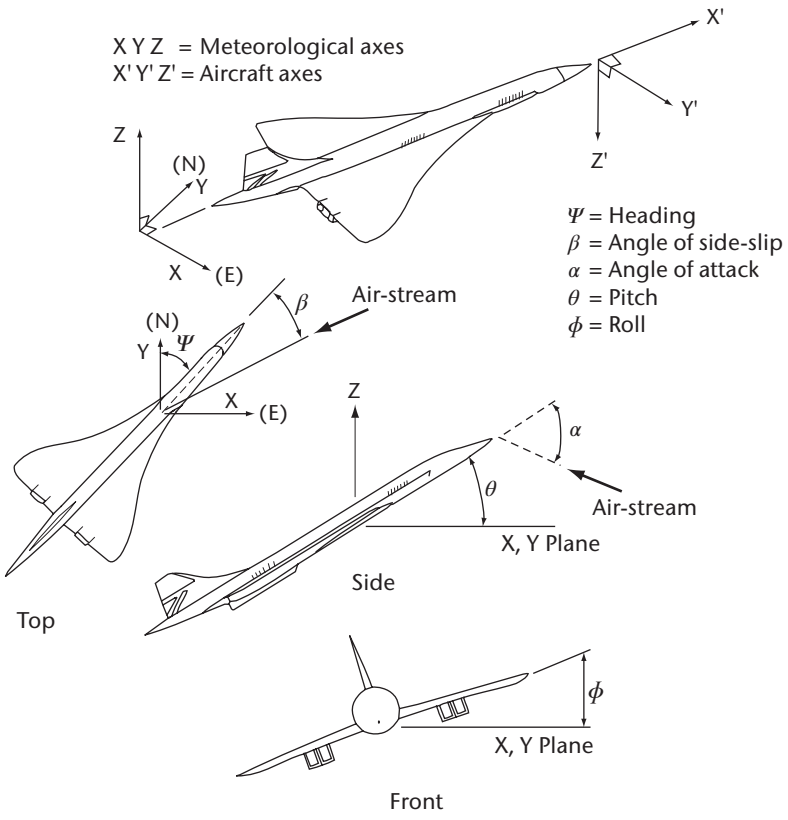

Figure 3.5. Angles between aircraft and the Earth's coordinate system as well as the air-stream

and yaw as well as the angle of attack and side-slip (Figure 3.5). In normal level flight, pitch and roll angle are very small and can be neglected. In the on-board system of a commercial aircraft, the wind vector triangle is only calculated in the X-Y plane of the Earth coordinate system and the angles of attack and side-slip are not measured.

The input data requirement reduces to true airspeed, heading and ground velocity. Heading and ground velocity are taken from the navigation system. True airspeed must be calculated from the Mach number and T_s. The components of the horizontal wind (u, v) are:

$$u = u_g - |\vec{v}_a| \cdot \sin\Psi \tag{3.8}$$

$$v = v_g - |\vec{v}_a| \cdot \cos\Psi \tag{3.9}$$

where $|\vec{v}_a|$ is the magnitude of the true airspeed; Ψ is the heading relative to true north, positive clockwise; and u_g and v_g are the components of the ground speed.

3.4.1 Measurement uncertainty

True airspeed is a function of the Mach number and T_s (SAT in Figure 3.1):

$$|\vec{v}_a| = 38.867 \cdot M \cdot \sqrt{T_s} \tag{3.10}$$

$$|\vec{v}_a| = 38.867 \cdot M \cdot \sqrt{\frac{T_r}{1 + 0.194 \cdot M^2}} \tag{3.11}$$

Since uncertainties exist in both Mach number and T_s, the total uncertainty of the true airspeed's magnitude is given by:

$$\Delta|\vec{v}_a| = 38.867 \cdot \Delta M \cdot \sqrt{T_s} + \frac{19.433 \cdot M \cdot \Delta T_s}{\sqrt{T_s}} \tag{3.12}$$

with $|\vec{v}_a|$ in units of kt; T_s, T_r in units of K; ΔM is the uncertainty of the Mach number; and ΔT_s is the uncertainty of the static temperature.

Note from equation 3.5 that Mach uncertainty depends on the uncertainty of the pressure measurements. Unless gross temperature errors exist, the Mach number uncertainty can be the most significant. For example, with a Mach number uncertainty of 0.2% at cruise level, airspeed uncertainty is some 1 kt (0.5 m/s). Thus, with zero uncertainty from the navigation system, wind vector uncertainty of up to 0.5 m/s is to be expected. Note, however, that gross temperature errors will lead to gross wind errors.

Uncertainty in true airspeed combines with uncertainty from the inertial reference unit. The basic calculations assume perfect alignment of the aircraft with the air-stream (no angle of side-slip) and zero roll and perfect inertial platform alignment. At high roll angles, wind vector uncertainty, which is proportional to true airspeed, can be significant. Roll angles of 10 to 20 degrees imply that the actual angle of attack makes an angular deviation of the true airspeed by a couple of m/s. So, wind data are usually excluded or at least flagged when the roll angle is above a threshold (typically 3 to 5 degrees). At low wind speeds, vector uncertainty can lead to large errors in wind direction. Thus, a more useful indication, considering all of the above uncertainty sources and combining wind speed and direction uncertainty as vector uncertainty, would suggest a typical uncertainty of 4–6 kt (2–3 m/s). These estimates are in line with operational experience (see, e.g., Nash, 1994).

3.5 HUMIDITY

Various sensor principles for the measurement of humidity are in use on research and operational commercial aircraft. The range of technologies covers capacitative-absorption, chilled mirrors and optical methods based on absorption or scattering. The instrument most widely used within AMDAR operations is one based on a tunable diode laser (TDL) (May, 1998; Fleming, 2000, 2003) – the Water Vapor Sensing System (WVSS-II). The TDL absorption spectroscopy technology was originally designed by NASA's Jet Propulsion Laboratory for use on missions to Mars, because it provides high accuracy and extreme stability of measurement over many years. WVSS-II is designed specifically for commercial aviation use in support of AMDAR, using a special relative narrowband absorption method at a suitable infrared line of the water vapour. The intensity of radiation at the detector is related to the emitted radiation by Beer's law such that:

$$I = I_0 \cdot e^{-k\,x\,\rho_w} \tag{3.13}$$

where I is the received signal; I_0 is the emitted signal; k is the mass attenuation coefficient; x is the path length; and ρ_w is the absolute humidity (density of water vapour) in the sensing volume. I_0, k and x are known properties of the system. A local pressure and temperature measurement enables the system to take account of the density of dry air ρ_d. The absorption is scanned over a narrowband of wavelengths around the H_2O line at 1.37 μm. The absolute humidity in the sampling volume is derived by use of the 2f method (May and Webster, 1993). The system's firmware finally converts the raw 2f signal together with coincident temperature and pressure measurements to the proper output parameter, the water vapour mass mixing ratio, m:

$$m = \frac{\rho_w}{\rho_d} \tag{3.14}$$

The sensor system is small enough for a manageable integration on commercial aircraft. Except for during possible phase transitions, m is conserved during the pressure and temperature shift from outside into the sensor probe. The generated value of the mixing ratio is suitable for reporting without knowledge of local pressure and temperature values. This is also convenient in numerical atmospheric models using specific humidity (numerically almost indistinguishable from m) as the input variable.

3.5.1 Measurement uncertainty

Up to 2012, some climate chamber assessments as well as flight tests of this spectrometric humidity measurement system have revealed two features of the instrument's performance: at measurement values above the detection limit of about 4 mg/m^3, the relative uncertainty is in the range of ±10%. At an altitude of 200 hPa, the corresponding detection limit in the mixing ratio is 0.02 g/kg (or 30 ppmv). Comparison of this aircraft-based method with contemporary radiosondes (see, e.g., Petersen et al., 2011), shows that the sensor appears to meet WMO observational requirements across all specific humidity and relative humidity ranges, during both ascent and descent.

3.6 TURBULENCE

Turbulence, especially clear-air turbulence (turbulence in the absence of clouds), is an important and potentially dangerous phenomenon in aviation. Although for routine commercial operations flight paths are designed to avoid turbulence, inevitably aircraft will experience unexpected bumpiness and the departure from normal level flight can be measured by the aircraft instrumentation.

3.6.1 Turbulence from vertical acceleration

Vertical acceleration (normal to the aircraft horizontal reference plane) is measured in the inertial reference unit. The data output is referenced and scaled to the acceleration due to gravity and may be categorized as shown in the table. However, the severity of turbulence affecting an aircraft depends principally on airspeed, the mass of the aircraft, the altitude and the nature of the turbulence itself. Hence, reports of turbulence from an aircraft derived from peak acceleration according to the crude relationships given in the table are of limited application and are aircraft-specific because a given gust will have different effects on different aircraft.

Example of coding for the scale of turbulence, defined by peak acceleration

Turbulence category	*Peak acceleration*[a]	*Code*
None	Less than 0.15 g	0
Light	0.15 g to, but not including, 0.5 g	1
Moderate	0.5 g to 1.0 g	2
Severe	Greater than 1.0 g	3

a These accelerations, which may be positive or negative, are departures from the normal acceleration of gravity (1.0 g).

3.6.1.1 *Measurement uncertainty*

There are two main sources of uncertainty in the aircraft instrumentation, namely the "zero", or reference, uncertainty and the output calibration (measurement) uncertainty. For most aircraft, the reference value is nominally +1.0 g, but this can vary typically by 3%. This uncertainty can be virtually eliminated by correction when the aircraft is on the ground, leaving a residual (including measurement) uncertainty of about 3% of measurement (Sherman, 1985).

3.6.2 Derived equivalent vertical gust velocity

An alternative indicator of turbulence is the derived equivalent vertical gust velocity (DEVG), defined as the instantaneous vertical gust velocity, which, superimposed on a steady horizontal wind, would produce the measured acceleration of the aircraft. The effect of a gust on an aircraft

depends on the mass and other characteristics, but these can be taken into account so that a gust velocity can be calculated which is independent of the aircraft. The derived equivalent vertical gust is given (Sherman, 1985) by:

$$U_{de} = \frac{Am\Delta n}{V_c} \tag{3.15}$$

where U_{de} is the derived equivalent gust velocity; Δn is the modulus of the peak deviation of the aircraft vertical acceleration from 1 g in units of g; m is the total mass; V_c is the calibrated airspeed at the time of the occurrence of the acceleration peak; and A is a parameter that depends on the aircraft type, and weakly on the mass, the altitude and the Mach number.

3.6.2.1 *Measurement uncertainty*

Uncertainties in each of the elements contributing to U_{de} have been estimated. These are typically less than 3% maximum for each element in normal level flight and in the extreme could lead to a total uncertainty of 10% to 12%. Assuming a random distribution of errors, a typical uncertainty would be 3% or 4% of the final value of U_{de}. Aircraft manoeuvres can also lead to large vertical accelerations of an aircraft, and, conversely, active control techniques can dampen the acceleration due to gusts, leading to serious underestimation of vertical gust velocities.

3.6.3 Eddy dissipation rate

The eddy dissipation rate, ε, is a parameter that quantifies the turbulence intensity within a fluid. In the context of aircraft turbulence, it is standard practice to refer to $\varepsilon^{1/3}$ as EDR. The advantage of EDR is that it is an aircraft-independent measure of the atmospheric turbulence intensity. There are several ways of estimating EDR (accelerometer-based versus wind-based), and they can be estimated, in principle, along any direction (though usually either vertical or longitudinal (along-track) is used). There are also different spectral models of turbulence that can be used for any of the algorithms:

$$F_v(f) = \frac{9\pi}{55V_t}\alpha\,\varepsilon^{2/3}\,L^{5/3}\,\frac{(1+\frac{32}{3}\pi^2L^2f^2/V_t^2)}{(1+4\pi^2L^2f^2/V_t^2)^{11/6}} \tag{3.16}$$

Equation 3.16 is the von Karman spectral model, where f is the frequency (Hz), V_t is the aircraft true airspeed (m/s), α is an empirical constant (taken here to be 1.6), and L is a length-scale parameter of the turbulence.

$$F_k(f) = \frac{24\pi}{55V_t}\alpha\,\varepsilon^{2/3}\left(2\pi f/V_t\right)^{-5/3} \tag{3.17}$$

Equation 3.17 is the Kolmogorov spectral model, which is just the high-frequency limit of equation 3.16. Both models attempt to describe the frequency power spectrum shape of wind data. The von Karman model better represents the larger scales, especially of the vertical velocity, though it is more complicated and includes the situation-dependent length scale L, in addition to EDR (squared). Research aircraft measurements have shown values of L from about 300 to 2 000 m. For most of the algorithm implementations to date, a mid-range value of 669 m is used.

3.6.3.1 *Vertical accelerometer-based EDR*

This method, described in Cornman et al. (1995), is based on the vertical-acceleration parameter available from the inertial navigation system. For this method, the following relation (Cornman et al., 1995, equation 21) is used:

$$\varepsilon_w^{1/3} = \frac{\hat{\sigma}_{\ddot{z}}}{\left[0.7V_t^{2/3}I(f_l,f_h)\right]^{1/2}} \tag{3.18}$$

where $\hat{\sigma}_{\ddot{z}}$ is the variance of the bandpass filtered vertical acceleration, I is the integral of the aircraft response bandpass filtered function H, and:

$$I(f_l, f_h) = \int_{f_l}^{f_h} \left| H_{\ddot{z}w}(f) \right|^2 \hat{S}_w(f) df \tag{3.19}$$

where $\hat{S}_w$ is the assumed Kolmogorov spectral model with $\varepsilon = 1$. The von Karman model could be substituted for the Kolmogorov. In the current implementation, f_l (stopband cut-off) and f_h (passband cut-off) are set to 0.1 Hz and 0.8 Hz, respectively. The purpose of the bandpass filter is to remove accelerations that are due to aircraft manoeuvres and wing bending mode frequencies rather than turbulence.

The aircraft response integral is evaluated for a range of flight conditions and stored in look-up tables, thus simplifying and reducing the on-board computation requirement. The algorithm calculates the running root-mean-square of the filtered signal over ten-second windows. At an 8 Hz sampling rate, this provides 480 EDR estimates per minute, from which the median and 90th percentile (referred to as the "peak") of these estimates are used for downlink. The EDR measurement results are converted into reporting numbers by use of tables which are far more detailed than that given in section 3.6.1. Extensive descriptions of these tables are given in the *Aircraft Meteorological Data Relay (AMDAR) Reference Manual* (WMO, 2003).

3.6.3.2 ***Vertical wind-based EDR***

This technique is briefly outlined in Cornman et al. (2004). The main idea is to compute the vertical winds directly, and then estimate the EDR from those calculations. This method has the advantage of not requiring the aircraft response function, which is difficult to obtain due to its proprietary nature.

$$w = V_T \left(\sin\alpha_b \cos\theta \cos\varphi - \cos\alpha_b \sin\theta \right) - \dot{Z} \tag{3.20}$$

The above equation is used to compute the vertical winds, where α_b is the body-axis angle of attack, θ is the pitch angle, φ is the roll angle, and $\dot{Z}$ is the inertial vertical velocity. EDR is computed by:

$$\hat{\varepsilon}^{1/3} = \left[\frac{1}{k_h - k_l + 1} \sum_{k=k_l}^{k_h} \frac{S^w(k)}{\hat{S}_w(k)} \right]^{1/2} \tag{3.21}$$

where k_l and k_h are index bounds corresponding to frequency bounds of 0.5 and 3.5 Hz (respectively) for the current 8 Hz implementations, S^w is the power spectrum of w (equation 3.20) after time-series processing, and $\hat{S}_w$ is the assumed von Karman spectral model with $\varepsilon = 1$, modified to account for various signal processing artefacts in S^w.

Nominally, the algorithm calculates EDR ($\varepsilon^{1/3}$) over ten-second windows, every five seconds. This provides 12 EDR estimates per minute, from which the actual mean and peak of these estimates are used for downlink. The mean and peak EDRs, along with quality-control metrics, are converted into reporting numbers by use of encoding (see section 5.3.13.5 in ARINC, 2012). The reported precision of both the mean and peak EDR is 0.02, significantly higher than in the accelerometer-based method.

3.6.3.3 ***True airspeed-based EDR***

This technique is similar to the vertical wind-based EDR (section 3.6.3.2) except that the spectral models are slightly different and true airspeed is used in place of w. The advantage of this method is that it is simpler to implement, requiring only one parameter. The disadvantage is that it estimates EDR mainly in the direction along the track, which has much less impact on the aircraft than from turbulence in the vertical direction.

3.6.3.4 *Measurement uncertainty*

As for DEVG, in the EDR there are potentially a large number of sources contributing to measurement uncertainty. Based on the analysis for DEVG, in the accelerometer-based method an uncertainty of some 5% to 10% can be expected for the mean, and somewhat larger for the peak. Based on simulations, similar performance is expected from the other EDR algorithms. A further complication arises over the choices of sampling interval and averaging time. Examination of typical time series of vertical acceleration data often indicates high variability of statistical properties over short distances. Variation of airspeed for a single aircraft alters the sampling distances.

3.6.3.5 *Relationship between EDR and DEVG*

Detailed field comparisons (Stickland, 1998) have been made between the accelerometer-based EDR and DEVG. These have shown a high correlation between peak EDR and DEVG for the same turbulence incidents. This result should be expected since the accelerometer-based EDR is directly proportional to the standard deviation of vertical acceleration over the measurement interval chosen. Hence, for a "normal" distribution, the extreme value will correlate closely with the peak vertical gust (proportional to the peak deviation of vertical acceleration). Clearly, this relationship will not apply to a singular event falling outside the assumed distribution, and the EDR filter cut-off at 0.8 Hz might well unduly attenuate very sharp gust events. For the vertical wind- and true airspeed-based methods, little filtering is applied, and it is not significantly susceptible to this last issue.

3.7 ICING

Several types of sensors may detect ice build-up on the flying surfaces. The following two types are in use:

(a) A thin-film capacitive sensor attached to the airfoil;

(b) A mechanical (vibrating-transducer) sensor exposed to the air-stream in a probe adjacent to the relevant flying surface.

3.7.1 Measurement uncertainty

The output of both sensors is essentially an "ice/no ice" signal, and uncertainty would be described by false-alarm rate. At present, no data are available on false-alarm rates for these sensors.

3.8 AIRCRAFT-BASED OBSERVING SYSTEMS

There are a number of operational aircraft-based observing systems in current operation. AMDAR is currently the major source of aircraft-based observations on the Global Telecommunication System; however, additional observations derived from other aircraft-based observing systems contribute significantly and are expected to provide increased data volumes in the future.

A number of AMDAR-like systems either have or are being developed which will improve global coverage and increase the number of observations in the boundary layer and lower troposphere. Some emphasis is being placed on recruiting smaller regional and general aviation aircraft to install either conventional AMDAR systems or dedicated sensor and communication systems. These aircraft operate from smaller airports that are not normally covered by existing AMDAR-reporting aircraft from airlines participating in national and regional AMDAR programmes.

3.8.1 Aircraft meteorological data relay

The AMDAR observing system should be operated according to WMO specification and standards (WMO, 2013). AMDAR is currently based and relies almost exclusively upon the Aircraft Communications Addressing and Reporting System (ACARS). AMDAR systems report data in profile (ascent/descent) mode as well as during level flight at cruise altitude.

For additional information on the regulatory requirements for establishment and operation of an AMDAR programme and the provision of other aircraft-based observations, consult the WMO *Manual on the Global Observing System*, Part III, 2.5 (WMO, 2010*a*), and the WMO *Guide to the Global Observing System*, Part III, 3.4 (WMO, 2010*b*).

For current information on operational AMDAR programmes and additional resource and guidance material, refer to the WMO AMDAR website: http://www.wmo.int/amdar.

3.8.2 Tropospheric Airborne Meteorological Data Reporting

3.8.2.1 *TAMDAR overview*

Tropospheric Airborne Meteorological Data Reporting (TAMDAR) is a commercially developed, deployed and operated system that derives and sells meteorological data derived from the predominantly aircraft-independent sensing and communications probe. Unlike in the WMO AMDAR observing system, in the TAMDAR system emphasis has been placed on equipping primarily regional carriers, as these flights tend to (i) fly into more remote and diverse locations, and (ii) be of shorter duration, thereby producing more daily vertical profiles and remaining in the boundary layer for longer periods. Although TAMDAR is fully functional and regularly operates above 40 000 ft, the aircraft that typically host the sensor often cruise below 25 000 ft.

TAMDAR collects measurements of relative humidity (RH), pressure, temperature, winds, icing and turbulence, along with the corresponding location, time and geometric altitude from a built-in GPS. These data are relayed via satellite in real time to a ground-based network operations centre, where in-line quality control procedures are performed prior to distribution. The overall humidity and temperature data quality is similar to that of radiosondes (Gao et al., 2012). The wind observations are derived in a similar fashion as typical AMDAR winds, using aircraft heading, true airspeed, and the ground track vector, which is provided by the internal GPS unit.

The TAMDAR sensor samples on a pressure-based interval on ascent and descent, and a time-based interval in cruise, which also varies with altitude from 3 min at lower altitudes to 7 min at higher altitudes. At present, on ascent and descent, the sensor reports every 10 hPa; however, this can be adjusted remotely in real time down to 1 hPa (~30 ft) depending on the rate of ascent and descent. During cruise, if any metric changes above a set threshold, the sensor will send a custom report, so turbulent flights through the cloud tops will generate far more observations than a higher-altitude cruise in clear skies.

3.8.2.2 *Relative humidity and temperature*

TAMDAR uses two capacitive sensing devices for redundancy to measure RH. The fundamental physical parameter that the TAMDAR capacitive sensor technology responds to is the density of H_2O molecules. RH is a derived parameter, which takes into account temperature and pressure. A custom hydrophobic membrane filter has been added to the devices, which significantly increases the reliability and accuracy by preventing direct wetting of the sensor element (see Mulally and Braid, 2009).

The reported RH value is a "consensus" value between the two devices that is determined by an algorithm in the ground processing system described in Anderson (2006). The system considers the value and quality of each sensor output. Typically, if both sensors are reporting similar values,

the consensus value is simply the average of the two. If the sensors disagree by more than 5%, and one is determined to be faulty using methods described in Anderson (2006) and Gao et al. (2012), then the errant sensor's value is flagged and not used in the mean RH calculation.

Certain corrections must be applied to the actual RH that the sensor is reporting. The primary corrections are because of the Mach heating and the difference in air pressure between the ambient conditions and the conditions observed by the sensor. The RH for a parcel of air with a given water vapour concentration is a function of both temperature and pressure. There are four major factors that contribute to the uncertainty of the measurement of true RH as is done in TAMDAR:

(a) The measurement uncertainty of the RH sensor itself (ΔRH);

(b) The uncertainty of the TAMDAR probe temperature (T_{probe}) measurement – via a platinum resistance temperature device;

(c) The measurement uncertainty of the calculated static air temperature (T_{static});

(d) The measurement uncertainty of the ratio of the static pressure (P_{static}) to the RH sensor pressure (P_{probe}).

The basic calculation necessary for static RH is described by:

$$\mathrm{RH}_{\mathrm{static}} = \mathrm{RH}_{\mathrm{probe}} \left(\frac{P_{\mathrm{static}}}{P_{\mathrm{probe}}} \right) \cdot \left(\frac{e_{s_{\mathrm{probe}}} \left(T_{\mathrm{probe}} \right)}{e_{s_{\mathrm{static}}} \left(T_{\mathrm{static}} \right)} \right) \tag{3.22}$$

where RH_{static} is the atmospheric RH, RH_{probe} is the actual RH measurement from the RH sensor in the TAMDAR probe, P_{static} is the static air pressure, P_{probe} is the air pressure at the RH sensor in the probe, T_{probe} is the temperature in the probe sensing cavity, T_{static} is the static air temperature, $e_{s,probe}$ is the probe saturation vapour pressure relative to water, and $e_{s,static}$ is the static saturation vapour pressure relative to water. The saturation pressure ratio is strictly a function of T_{probe} and T_{static} as shown above. The calculation for the pressure ratio (P_{static}/P_{probe}) has been derived from data from extensive wind tunnel testing (see Braid et al., 2011; Smith et al., 2012).

The relationship between T_{probe} (essentially the recovered temperature) and T_{static} is:

$$T_{\mathrm{probe}} = T_{\mathrm{static}} (1 + \lambda \cdot M^2) \tag{3.23}$$

where M is the Mach number and λ is a constant approximately equal to 0.17. The actual RH sensor measurement is the true value plus a sensor uncertainty, ΔRH, thus:

$$\mathrm{RH}_{\mathrm{probe}} = \mathrm{RH}_{\mathrm{true}} + \Delta \mathrm{RH} \tag{3.24}$$

Substituting equation 3.24 into equation 3.22 illustrates an issue that needs consideration when using the RH method. As the Mach number increases and the temperature decreases, the saturation pressure ratio ($e_{s,probe}/e_{s,static}$) in equation 3.22 increases rapidly, and, as a result, the effect of the sensor uncertainty, ΔRH, is amplified. The ground processing system estimates the error in the RH based on temperature and Mach. This is used along with the known accuracy of the RH sensor and the temperature accuracies to calculate an overall RH uncertainty, which is reported along with the RH.

The range of RH that will be experienced by the RH sensor is also reduced due to the Mach heating. At high speeds, the RH internal to the probe will generally be less than 10% due to the Mach heating of the air. This effect is addressed in TAMDAR by the calibration process. Each RH sensor is characterized over several RH and temperature conditions. Values are specifically chosen at conditions which are error prone, in particular cold, dry conditions. This calibration process results in an RH measurement capability that is useful even at high altitudes. It should be mentioned that one effect of Mach heating is beneficial. Since the response of the capacitive sensor slows down as temperature decreases, the Mach heating effect keeps the RH sensor significantly warmer than ambient, resulting in a response time much faster than otherwise.

3.8.2.3 *TAMDAR icing detection*

The TAMDAR sensor detects icing using two light-emitting diode (LED) and photo detector (PD) pairs, each having an associated analogue-to-digital converted (AtDC) voltage output value. When a TAMDAR sensor encounters conditions where icing is present, ice accumulates on the surface of the foil gap in the area between the LED/PD pairs. As the thickness of the ice increases, the infrared beams become obscured, dropping the AtDC values of the LED/PD pairs below half of the nominal unblocked value, which results in a positive icing indication within the TAMDAR sensor. Once the detection of ice is confirmed via algorithms that verify consistency of the event with current environmental conditions (that is, T and RH), the TAMDAR probe heaters are automatically activated to remove the ice. This process continues until the PD voltage values are greater than half the nominal unblocked value.

All icing events experienced by TAMDAR are tracked in the data stream with the use of icing flags. These flags track the initiation of the icing event, the time at which the heaters were activated, the period of continued icing, the probe cool-down, and when icing is no longer present. The AtDC values of the LED/PD pairs, which are used to detect the presence or absence of icing, are used to calculate TAMDAR liquid water content (LWC). The resulting rate of change in the TAMDAR AtDC voltage output is used to calculate accretion rate, and this is the basis for obtaining LWC values. The temporal drop rate of AtDC values is used to calculate the icing intensity or accretion rate.

3.8.2.4 *TAMDAR turbulence detection*

Turbulence is reported as an eddy dissipation rate and is based on true airspeed (TAS) samples which are calculated from the TAMDAR pitot and static port pressures and the TAMDAR temperature. The report includes the mean and peak EDR, and the time of peak for each one minute period. The EDR turbulence algorithm is independent of aircraft configuration and flight condition. Thus, it does not depend on the type of aircraft or on load and flight capacity.

The TAMDAR methodology utilizes an estimate of the longitudinal wind via the TAS parameter to calculate EDR. TAMDAR can obtain TAS via two sources: (i) from the TAMDAR static and pitot pressure sensor measurements or (ii) from the aircraft's ARINC 429 databus. Once the system takes a measurement of the differential pressure between the pitot and static pressure, the measure is then passed through a filter before TAS is calculated.

The MacCready method is used to estimate the EDR based on the expected –5/3 power spectra slope from the Kolmogorov model of the TAS signal. The filtering of the differential pressure sensor uses a low-pass Butterworth anti-alias filter, with 4th order 5 Hz 3 decibel cut-off frequencies. Windowing is completed prior to fast Fourier transformation (FFT) to make the measurement more spectral (64 point FFT). An EDR is calculated every 3 s using a 6 s block of 10.67 Hz TAS data. EDR values can be averaged if desired for a smoother result; normally a 6 s average is used, but users have the ability to configure this averaging to match their needs. A quality assurance filter is also employed.

3.9 OTHER SYSTEMS AND SOURCES OF AIRCRAFT-BASED OBSERVATIONS

3.9.1 ICAO Automatic Dependent Surveillance

The development of global air navigation systems is closely linked to developments in communication systems. Thus, the Future Air Navigation System (FANS) is coupled with the development of an Automatic Dependent Surveillance (ADS) system which itself is dependent on global satellite aircraft communication. The global aircraft communication system is migrating to an open network under the Aeronautical Telecommunication Network project (Wells et al., 1990). This will link the VHF and Satcom Systems into a common open network.

The successful weather routing of commercial aircraft, especially to provide flight safety, minimize fuel consumption and airframe fatigue, and to ensure passenger comfort, demands greater accuracy in aviation forecasts. Hence, automatic reports of aircraft position for ADS allow for the inclusion of automated meteorological reports. The data to be included in these reports are essentially the same as those of current AMDAR systems including allowance for turbulence and humidity elements.

Data derived from the ICAO ADS contract (ADS-C) system are being transmitted on the WMO Global Telecommunication System. These data are made available through the arrangement established with ICAO as set out in ICAO Annex 3 to the Convention on International Civil Aviation, *Meteorological Service for International Air Navigation*, Chapter 5 and Appendix 4. ICAO regulations stipulate that air traffic management centres are to transmit the ADS-C messages to the World Area Forecast Centres (WAFCs), which are then responsible for transmission of the data on the Global Telecommunication System (see *Procedures for Air Navigation Services – Air Traffic Management*, ICAO Doc. 4444, 4.11.4).

3.9.2 New and developing systems

3.9.2.1 *Mode-S Enhanced Surveillance*

Wind and temperature observations can also be inferred from surveillance data gathered for air traffic control (ATC) purposes using a Mode-S(elective) Enhanced Surveillance (EHS) radar. This radar interrogates every aircraft for specific information at a frequency rate of 4 to 20 s, depending on the ATC purposes of the radar. In designated airspace, all aircraft are obliged to respond to the interrogation by the Mode-S EHS radar. The mandatory registers (BDS4,0, BDS5,0 and BDS6,0) contain information on aircraft identity, flight level, roll angle, magnetic heading, airspeed, Mach number and ground track. Position of the aircraft can be obtained either from the ATC radar or from the Automatic Dependent Surveillance Broadcast (ADS-B) data which are transmitted continuously by the aircraft.

The derivation of wind from Mode-S EHS is similar to AMDAR, except that the true heading has to be determined from the magnetic heading. Besides applying a magnetic variance table, additional aircraft-dependent corrections need to be applied. Heading corrections may change with time due to maintenance of the aircraft. At present these corrections are determined for every aircraft based on comparison with numerical weather prediction (NWP) data. Next to the heading correction, an airspeed correction is applied also based on long-term comparison with NWP data (see de Haan, 2013). After corrections and quality control, the derived wind information is of similar quality as from AMDAR (de Haan, 2011, 2013). The derivation of temperature from Mode-S EHS observations is done by combining the Mach number and the airspeed. The quality of the derived temperature is hampered by the reported resolution of the Mach number and airspeed, and is clearly of less quality than AMDAR temperature (de Haan, 2011, 2013).

3.9.2.2 *Mode-S Meteorological Routine Air Report*

A Mode-S EHS radar can also interrogate non-mandatory registers which may contain meteorological information. An example is the Mode-S EHS BDS4,4 register, called Meteorological Routine Air Report (MRAR). This register contains direct wind and temperature information which is very close to the AMDAR wind and temperature information (Stranjar, 2012). Since the register BDS4,4 is not mandatory, only a fraction (about 5%) of the aircraft respond to the request with valuable meteorological information.

REFERENCES AND FURTHER READING

Abbott, I.H. and A.E. von Doenhoff, 1959: *Theory of Wing Sections*. Dover Publications, Inc., Mineola, New York, 693 pp.

AirDat, 2003: *TAMDAR – Tropospheric Airborne Meteorological Data Reporting Sensor and System Overview; AirDat Infrastructure and Global Capabilities*. Information document, AirDat LLC, Evergreen, Colorado.

Anderson, A.K., 2006: *AirDat system for ensuring TAMDAR data quality*. Tenth Symposium on Integrated Observing and Assimilation Systems for the Atmosphere, Oceans, and Land Surface (IOAS-AOLS), American Meteorological Society, Atlanta, GA.

ARINC, 2012: *620-7 Data Link Ground System Standard and Interface Specification*. Aeronautical Radio, Inc., Annapolis, Maryland.

Benjamin, S.G., B.D. Jamison, W.R. Moninger, S.R. Sahm, B.E. Schwartz and T.W. Schlatter, 2010: Relative short-range forecast impact from aircraft, profiler, radiosonde, VAD, GPS-PW, METAR, and Mesonet observations via the RUC hourly assimilation cycle. *Monthly Weather Review*, 138:1319–1343.

Braid, J., P. Van Wie and J. Rex, 2011: Using the TAMDAR sensor for in-flight ice detection and improved safety of flight. *SAE Technical Paper 2011-38-0051*, International Conference on Aircraft and Engine Icing and Ground Deicing, Society of Automotive Engineers.

Cornman, L.B., G. Meymaris and M. Limber, 2004: *An update on the FAA Aviation Weather Research Program's in situ turbulence measurement and reporting system*. Eleventh Conference on Aviation, Range and Aerospace Meteorology, Hyannis, MA.

Cornman, L.B., C.S. Morse and G. Cunning, 1995: Real-time estimation of atmospheric turbulence severity from in situ aircraft measurements. *Journal of Aircraft*, 32(1):171–177.

Dommasch, D.O., S.S. Sherby and T.F. Connolly, 1958: *Airplane Aerodynamics.* New York, Pitman, 560 pp.

Fleming, R.J., 2000: Water vapor measurements from commercial aircraft: Progress and plans. *Preprints*. Fourth Symposium on Integrated Observing Systems, Long Beach, CA, American Meteorological Society, 30–33.

———, 2003: The WVSS-II and the UCAR air sampler: Purpose, design, status (personal communication). University Corporation for Atmospheric Research, Boulder, Colorado.

Gao, F., X.Y. Zhang, N.A. Jacobs, X.-Y. Huang, X. Zhang and P.P. Childs, 2012: Estimation of TAMDAR observational error and assimilation experiments. *Weather and Forecasting*, 27:856–877.

Haan, S. de, 2011: High-resolution wind and temperature observations from aircraft tracked by Mode-S air traffic control radar. *Journal of Geophysical Research*, 116(D10111).

———, 2013: *An Improved Correction Method for High Quality Wind and Temperature Observations Derived from Mode-S EHS*. KNMI Technical Report No. TR-338, De Bilt.

International Civil Aviation Organization (ICAO), 2007: *Procedures for Air Navigation Services – Air Traffic Management*. Fifteenth edition, Doc 4444, Montreal.

———, 2013: *Meteorological Service for International Air Navigation*. ICAO Annex 3, Eighteenth edition, Amendment 76, Montreal.

International Organization for Standardization (ISO), 2007: *Standard Atmosphere*, ISO 2533:1975 (with two additions in 1985 and 1997, reviewed and confirmed in 2007). Geneva.

Lawson, R.P. and W.A. Cooper, 1990: Performance of some airborne thermometers in clouds. *Journal of Atmospheric and Oceanic Technology*, 7:480–494.

May, R.D., 1998: Open-path, near-infrared tuneable diode laser spectrometer for atmospheric measurements of H_2O. *Journal of Geophysical Research*, 103:19161–19172.

May, R.D. and C.R. Webster, 1993: Data processing and calibration for tuneable diode laser harmonic absorption spectrometers. *Journal of Quantitative Spectroscopy and Radiative Transfer*, 49(4):335–347.

Meteorological Service of Canada, 2003: *The Effect of Pitch and Roll Attitude on the Calculation of Wind* (G. Bruce). Aeromechanical Services Ltd., 1118-1c, Rev. 1.0.

Moninger, W.R., S.G. Benjamin, B.D. Jamison, T.W. Schlatter, T.L. Smith and E.J. Szoke, 2010: Evaluation of regional aircraft observations using TAMDAR. *Weather and Forecasting*, 25:627–645.

Mulally, D.J. and J.T. Braid, 2009: *The TAMDAR Sensor's Relative Humidity Performance on ERJ-145 Commercial Aircraft*. Thirteenth Symposium on Integrated Observing and Assimilation Systems for the Atmosphere, Oceans, and Land Surface (IOAS-AOLS), American Meteorological Society, Phoenix, AZ.

Nash, J., 1994: Upper wind observing systems used for meteorological operations. *Annales Geophysicae*, 12:691–710.

Petersen, R.A., L. Cronce, W. Feltz, E. Olson and D. Helms, 2011: *Validation Studies of WVSS-II Moisture Observations*. Fifteenth Symposium on Integrated Observing and Assimilation Systems for the Atmosphere, Oceans, and Land Surface (IOAS-AOLS), American Meteorological Society, Seattle, WA.

Rodi, A.R. and P.A. Spyer-Duran, 1972: Analysis of time response of airborne temperature sensors. *Journal of Applied Meteorology*, 11:554–556.

Sherman, D.J., 1985: *The Australian Implementation of AMDAR/ACARS and the Use of Derived Equivalent Gust Velocity as a Turbulence Indicator.* Structures Report No. 418, Department of Defence, Defence Science and Technology Organisation, Aeronautical Research Laboratories, Melbourne, Victoria.

Smith, W.L., P. Minnis, C. Fleeger, D. Spangenberg, R. Palikonda and L. Nguyen, 2012: Determining the flight icing threat to aircraft with single-layer cloud parameters derived from operational satellite data. *Journal of Applied Meteorology and Climatology*, 51:1794–1810.

Stickland, J.J., 1998: *An Assessment of Two Algorithms for Automatic Measurement and Reporting of Turbulence from Commercial Public Transport Aircraft*. A report to the ICAO METLINK Study Group. Observations and Engineering Branch, Bureau of Meteorology, Melbourne.

Stickney, T.M., M.W. Shedlov, D.I. Thompson, 1990: *Rosemount Total Temperature Sensors*. Technical Report 5755, Revision B, Rosemount Inc.

Strajnar, B., 2012: Validation of Mode-S Meteorological Routine Air Report aircraft observations. *Journal of Geophysical Research: Atmospheres*, 117(D23).

Wells, V.E. et al., 1990: Migration of ACARS to the Aeronautical Telecommunication Network. *Proceedings of the Aeronautical Telecommunications Symposium on Data Link Integration*, Annapolis, Maryland.

World Meteorological Organization, 2003: *Aircraft Meteorological Data Relay (AMDAR) Reference Manual* (WMO-No. 958). Geneva.

———, 2010*a*: *Manual on the Global Observing System* (WMO-No. 544), Volume I. Geneva.

———, 2010*b*: *Guide to the Global Observing System* (WMO-No. 488). Geneva.

———, 2011: *Manual on Codes* (WMO-No. 306), Volume I.1. Geneva.

———, 2013: *AMDAR Onboard Software Functional Requirements Specification.* Instruments and Observing Methods Report No. 114. Geneva.